PCCP

ROYAL SOCIETY OF CHEMISTRY

PAPER

Cite this: *Phys. Chem. Chem. Phys.*, 2022, **24**, 20294

Computational investigation of van der Waals corrections in the adsorption properties of molecules on the Cu(111) surface†

Eduardo O. Bartaquim, [a] Raquel C. Bezerra, [b] Albert F. B. Bittencourt [c] and Juarez L. F. Da Silva *[a]

Received 12th June 2022,
Accepted 3rd August 2022

DOI: 10.1039/d2cp02663e

rsc.li/pccp

Here, we report a computational investigation on the role of the most common van der Waals (vdW) corrections (D2, D3, D3(BJ), TS, TS+SCS, TS+HI, and dDsC) employed in density functional theory (DFT) calculations within local and semilocal exchange–correlation functionals to improve the description of the interaction between molecular species and solid surfaces. For this, we selected several molecular model systems, namely, the adsorption of small molecules (CH_3, CH_4, CO, CO_2, H_2O, and OH) on the close-packed Cu(111) surface, which bind *via* chemisorption or physisorption mechanisms. As expected, we found that the addition of the vdW corrections enhances the energetic stability of the Cu bulk in the face-centered cubic structure, which contributes to increasing the magnitude of the mechanical properties (elastic constants, bulk, Young, and shear modulus). Except for the TS+SCS correction, all vdW corrections substantially increase the surface energy, while the work function changes by about 0.05 eV (largest change). However, we found substantial differences among the vdW corrections when comparing its effects on interlayer spacing relaxations. Based on bulk and surface results, we selected only the D3 and dDsC vdW corrections for the study of the adsorption properties of the selected molecules on the Cu(111) surface. Overall, the addition of these vdW corrections has a greater effect on weakly interacting systems (CH_4, CO_2, H_2O), while the chemisorption systems (CH_3, CO, OH) are less affected.

1 Introduction

The adsorption of molecular species on transition-metal substrates plays a critical role in improving our atomistic understanding of a wide range of chemical reactions, in particular the identification of adsorption modes and active sites on catalysts.[1,2] The binding of molecular species on substrates can be characterized by the formation of chemical bonds (chemisorption, eV magnitude)[3] or physical bonds (physisorption, fraction of eV),[3] for which the adsorption energies are of significantly different magnitudes. These interaction mechanisms have been recognized for decades, however, a quantitative description of these interactions remains a challenge for theoretical approaches,[4] particularly density functional theory (DFT) calculations employing local and semilocal exchange–correlation (XC) functionals.

Although exact, in principle, practical applications of DFT in computational physics, chemistry, and materials science require approximations for the XC energy functional.[5–7] Local and semilocal approximations, such as the local density approximation (LDA) or the generalized gradient approximation (GGA), have limitations in providing an accurate description of weak binding systems, *e.g.*, physisorption interactions, in which the long-range van der Waals (vdW) interactions are significant, whereas the description of chemisorption cases is less complicated but not entirely problem-free.

Local and semilocal XC functionals cannot provide an accurate description of vdW interactions for two primary reasons: (i) the XC functional does not describe the origin of the dispersion forces, which are instantaneous electronic density fluctuations; (ii) the functional only describes local properties, while vdW forces are a nonlocal phenomenon.[7] One approach to account for dispersion forces is the development of a nonlocal XC functional. These include vdW-DF by Dion *et al.*[8] and vdW-DF2 by Lee *et al.*[9] Additional methods for accounting

[a] *São Carlos Institute of Chemistry, University of São Paulo, P.O. Box 780, 13560-970, São Carlos, SP, Brazil. E-mail: juarez_dasilva@iqsc.usp.br*
[b] *Secretaria de Estado de Educação e Qualidade do Ensino (SEDUC) do Estado do Amazonas, Escola Áurea Pinheiro Braga Av. Perimentral, s/n, Lot. Cidade do Leste, Gilberto Mestrinho, 69089-340, Manaus, AM, Brazil*
[c] *School of Chemical Engineering, University of Campinas, 13083-970, Campinas, SP, Brazil*

† Electronic supplementary information (ESI) available: Details on the PAW projectors, computational convergence tests, vdW corrections, and all data used for the figures. Additional technical details are available upon request from the authors. See DOI: **https://doi.org/10.1039/d2cp02663e**

for vdW forces are based on the observation that these interactions exhibit exponential decay of $1/r^6$. Thus, it is conceivable to add a component with this decay adjusted by a dispersion coefficient (C_n^{AB}) to the DFT total energy.

In the past decade, several vdW corrections have been proposed to improve the description of weak interacting physisorption systems. The progress has been remarkable, and it is common to find several vdW corrections within the most common DFT implementations, *e.g.*, Grimme's D2,[10] Grimme's D3,[11,12] Grimme's D3 correction with Becke–Jonson damped function (D3(BJ)),[13] Tkatchenko–Scheffler (TS),[14] Tkatchenko–Scheffler with self-consistent screening (TS+SCS),[15] Tkatchenko–Scheffler with iterative Hirshfeld partitioning (TS+HI),[16,17] and density-dependent dispersion corrections (dDsC).[18,19] Consequently, it raises several questions regarding the optimal correction or approach to use when performing a computational study for a particular surface science topic requiring the description of bulk, clean surface, and adsorption properties. Therefore, the purpose of this study is to enhance our atomistic understanding of the effects of the most common vdW corrections for a set of particular molecular systems.

In order to evaluate the impact of vdW corrections on the adsorption properties of the Cu(111) surface, we selected six distinct adsorbates, including non-polar molecules (CH_4 and CO_2), polar molecules (CO and H_2O), and radicals (CH_3 and OH). Compared to other Cu surfaces, the close-packed Cu(111) surface exhibits the lowest surface energy due to the lower number of broken bonds.[20] Furthermore, the Cu metal surface was selected because copper-based catalysts are highly promising materials for organic synthesis[21,22] and the direct oxidation of methane to methanol.[23,24]

In this investigation, we found that vdW corrections play a significant role in the bulk properties of bulk Cu in the face-centered cubic (fcc) structure by increasing the mechanical properties and decreasing the lattice constant, which can be explained by the enhancement of the magnitude of the cohesion energy. Using the d-band center model, we also observed that the vdW interactions reduce the surface Cu(111) stability slightly. Furthermore, we identified that the site preference for adsorption can change with the vdW corrections, as the geometry of the chemical system affects the dispersion corrections differently.

2 Theoretical approach and computational details

2.1 Total energy calculations

All total energy calculations were carried out using the spin-polarized DFT[25,26] framework, as implemented in the Vienna *ab initio* simulation package (VASP),[27–29] version 5.4.4, within the Perdew–Burke–Ernzerhof (PBE)[30] formulation for the XC energy functional. To solve the Kohn–Sham (KS) equations, we employed the all-electron projector augmented-wave (PAW) method,[29,31] where the KS states are described by plane-waves. To obtain the equilibrium volume and elastic constants for the bulk Cu in the fcc structure, we used a plane-wave cutoff energy of 834 eV and a Monkhorst–Pack[32] **k**-mesh of 19 × 19 × 19 for the Brillouin zone (BZ) integration. For the remaining properties, which are less sensitive to the number of plane-waves, we used a cutoff energy of 469 eV, which is 12.5% higher than the maximum cutoff energy recommended for the oxygen projector.

For surface calculations, we used the repeated slab geometry with a slab thickness of 9 layers and 16 Å for the vacuum region. To sample the BZ of the (1 × 1) surface unit cell, we used a **k**-mesh of 20 × 20 × 1, which was increased to 30 × 30 × 1 for density of state calculations. A (3 × 3) surface unit cell was used for adsorption calculations and the **k**-mesh was reduced to 6 × 6 × 1 due to the smaller size of the BZ. To take advantage of the inversion symmetry present in the Cu(111) surface, the adsorbates were placed on both sides of the slab, and therefore no dipole corrections were required.

For free-atom and gas-phase molecule calculations, we used an orthorhombic box with dimensions of 19.50 Å × 19.75 Å × 20.00 Å. Due to the lack of dispersion in the electronic states within the BZ, only the Γ-point was considered for the BZ integration. For all bulk and surface calculations, equilibrium structures were obtained once the atomic forces on each atom were less than 0.025 eV $Å^{-1}$, with a criterion of 10^{-6} eV for the total energy convergence.

2.2 van der Waals corrections

As mentioned in the Introduction, a well-known drawback of local and semilocal XC energy functionals is the lack of precision to describe weak long-range vdW interactions, which can be explained by limitations in the description of the instantaneous electron density fluctuations.[5,7] Nevertheless, vdW interactions play a critical role in the modeling of molecular adsorption phenomena on metal surfaces,[1,33] affecting numerous studies in computational materials science.[7] To overcome these limitations, several vdW corrections have been proposed over the years, such as Grimmes's family D2,[10] D3,[11,12] and D3(BJ),[13] or corrections based on the Tkatchenko–Scheffler formulations such as TS,[14] TS+SCS,[15] and TS+HI,[16,17] or yet corrections based on the Becke–Johnson XC hole formulation such as the dDsC correction.[18,19]

For all listed vdW corrections, the total energy is obtained by the sum of the total DFT energy ($E_{\text{tot}}^{\text{DFT}}$) and the additive contribution of the vdW energy ($E_{\text{energy}}^{\text{vdW}}$), *i.e.*,

$$E_{\text{tot}} = E_{\text{tot}}^{\text{DFT}} + E_{\text{energy}}^{\text{vdW}}. \quad (1)$$

All vdW corrections listed above take the form of

$$E_{\text{energy}}^{\text{vdW}} = \sum_{AB} \sum_{n=6,8} s_n \frac{C_n^{AB}}{R_{AB}^n} f_{\text{d},n}(R_{AB}), \quad (2)$$

where R_{AB}^n is the distance between atoms A and B, $f_{\text{d},n}$ (R_{AB}) is a dumping function needed to avoid divergence caused by small values of R_{AB}^n, C_n^{AB} is a dispersion coefficient, and s_n is a global scaling factor that depends on the XC functional and the vdW correction method. The main difference between the vdW corrections considered in this work is in the terms C_n^{AB} and $f_{\text{d},n}$ (R_{AB}).

Grimme's D2 approach,[10] for example, is a semiempirical method in which the dispersion coefficient is determined by

the ionization potential and static polarizability of isolated atoms (obtained with hybrid DFT-PBE0 calculations). Despite its simplicity, the D2 methodology works for a wide range of scenarios;[7] however, this scheme has certain limitations because the dispersion coefficient remains constant regardless of the chemical environment.[7] In the case of D3, the chemical environment is evaluated based on the atomic coordination number. This can be accomplished by first determining the dispersion coefficient between two atoms in distinct chemical environments. Then, C_n^{AB} is calculated by interpolating the pre-calculated dispersion coefficients using a function that determines the number of neighbors.[7,12] To further improve the D3 scheme, this method can be combined with the Grimme *et al.* damping function, yielding the D3(BJ) vdW correction.[13]

To compensate for environmental sensitivity, the TS methodology uses effective atomic volumes,[14] but it cannot take into account screening effects. The TS+SCS correction attempts to address this limitation by computing frequency-dependent polarizabilities using the self-consistent screening equation.[15] When electrostatic effects and dispersion interactions are comparable, the TS method also fails. To address this, the Hirshfeld interactive scheme of the TS+HI approach could be used.[16,17] The dDsC methodology also accounts for chemical dependence on the environment; however, this is accomplished using the Becke–Johnson simplified XC dipole moment formalism.[18,19,34]

Despite the inclusion of chemical dependence on the environment, there are still issues that methods beyond the D2 scheme cannot solve.[7,15–17] Grimme's D3 methodology is based on the coordination number rather than the electronic structure, which is a source of calculation errors.[12] In addition to the problems already mentioned, the selection of neutral atoms is a major source of error in the TS approach.[7,15–17] Furthermore, because all of these approaches are physical models, they all have issues.[19] In the dDsC scheme, for example, all the derivatives of density-dependent parameters are set to zero, resulting in certain errors. Additional details on vdW corrections are discussed in the ESI,† Section S2.

2.3 Adsorbed structure configurations

Several high-symmetry adsorption sites, including top, bridge, hollow fcc, and hollow hcp sites, are present on the Cu(111) surface, as depicted in Fig. 1. Thus, for all adsorbates, namely CH_3, CH_4, CO, CO_2, OH, and H_2O, we initially considered their adsorption at each site approximately 2 Å above the surface. Different orientations were also investigated, *e.g.*, for CH_4, one hydrogen atom was placed above the C atom, while the remaining three hydrogen atoms were positioned at the bridge site for the case of the top configuration, *etc.* All configurations were relaxed without constraints for geometric relaxation.

3 Results and discussion

As mentioned above, the purpose of all vdW corrections is to improve the DFT-PBE description; however, a number of negative and positive factors can influence their selection for a particular application. In the following, we will summarize and discuss the key findings based on various vdW corrections implemented within VASP.

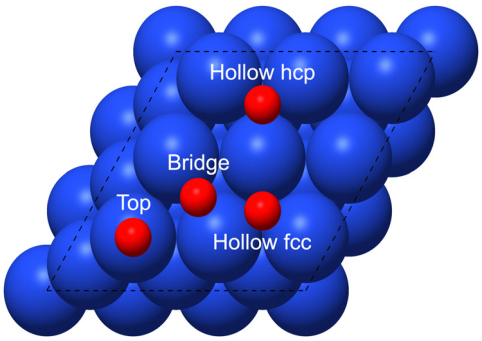

Fig. 1 Top view representation of the Cu(111) surface using a (3 × 3) surface unit (dashed lines). The red spheres represent the most important high-symmetry adsorption sites (top, bridge, hollow fcc, and hollow hcp).

3.1 Bulk properties

The bulk properties are summarized in Table 1, while Fig. 2 depicts their relative changes with respect to the PBE results. The effect of vdW corrections on the lattice constant, cohesion energy, and mechanical properties is discussed below.

3.1.0.1 Equilibrium lattice constant. Compared with the experimental measurement,[35] the equilibrium lattice constant (a_0) calculated using PBE is overestimated by 0.40%. As expected, the addition of vdW corrections into the DFT-PBE framework decreased the value of the equilibrium lattice. This is consistent with the attractive nature of the vdW interactions, which contributes to the shortening of the bond lengths in the bulk structure. By adding the vdW correction, the agreement with the experimental data worsens as the lattice constant becomes underestimated by approximately 2.0%. The TS vdW correction yielded the largest deviations from PBE (Fig. 2), followed by Grimme's corrections and the dDsC scheme. The exception was PBE+TS+SCS, which was closer to PBE than the other corrections.

3.1.0.2 Cohesion energy. Cohesion energy (E_{coh}) is the energy required to take atoms in their free form and join them to form a crystal, expressed as:

$$E_{coh} = E_{tot}^{bulk} - E_{tot}^{free\ atom}, \quad (3)$$

where E_{tot}^{bulk} is the total energy of the crystal structure and $E_{tot}^{free\ atom}$ is the free-atom total energy. Consistent with the experimental data given in Young's handbook,[36] all calculated values for E_{coh} were negative, indicating that the formation of the Cu crystal is an energetically favored process. The discrepancy between the PBE-determined and the experimental values is 0.62%. The use of vdW corrections decreased the value of E_{coh}, which is also consistent with the attractive nature of vdW interactions. With the exception of PBE+TS+SCS, TS vdW corrections produce the greatest variations from PBE, followed by Grimme's corrections and the dDsC scheme. The

Table 1 Effect of the vdW corrections on the bulk properties of Cu in the fcc structure: equilibrium lattice constant (a_0), cohesion energy (E_{coh}), elastic constants (C_{11}, C_{12}, C_{44}), bulk modulus (B), Young's modulus (E), and shear modulus (G)

DFT	a_0 (Å)	E_{coh}	C_{11} (GPa)	C_{12} (GPa)	C_{44} (GPa)	B (GPa)	E (GPa)	G (GPa)
PBE	3.630	−3.502	168.74	125.10	73.20	139.65	140.32	52.65
PBE+D2	3.565	−3.920	180.88	136.28	83.62	151.15	156.83	59.09
PBE+D3	3.563	−4.013	203.82	141.43	87.21	162.23	171.57	64.81
PBE+D3(BJ)	3.563	−4.094	200.98	147.56	93.35	165.37	176.37	66.69
PBE+TS	3.542	−4.115	206.31	156.26	101.42	172.94	187.04	70.86
PBE+TS+SCS	3.602	−3.858	164.08	145.28	69.18	151.54	123.51	45.27
PBE+TS+HI	3.544	−4.102	209.18	158.46	103.64	175.37	190.75	72.33
PBE+dDsC	3.590	−3.828	190.00	141.18	84.50	157.45	160.81	60.46
Expt.	3.615[35]	−3.480[36]	168.3[37]	122.1[37]	75.7[37]	142.06[38]	130[38]	47.9[39]

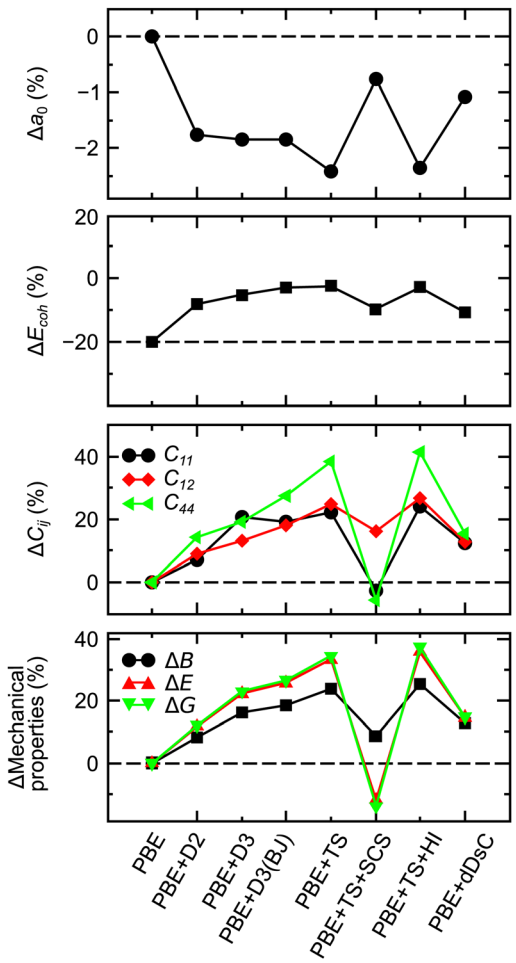

Fig. 2 Relative changes in the bulk Cu properties compared with the PBE results: equilibrium lattice constant (Δa_0), cohesive energy (ΔE_{coh}), elastic constants (ΔC_{ij}), bulk modulus (ΔB), Young's modulus (ΔE), and shear modulus (ΔG). The dashed lines indicate the PBE values, respectively.

variations from PBE, on the other hand, were greater than those from a_0, ranging from 9.31% for dDsC to 17.53% for PBE+TS.

3.1.0.3 Elastic constants. The discrepancy between the PBE-calculated and the experimental values for the elastic constants ranges from 2.40% to 3.41%. The use of the vdW corrections enhanced the magnitude of the elastic constants, with the exception of the TS+SCS scheme, where ΔC_{11} and ΔC_{44} were negative. These observations are also consistent with the attractive nature of the vdW interactions. Tkatchenko–Scheffler corrections produced the greatest deviations from PBE, followed by Grimme's corrections and dDsC corrections, with the exception of PBE+D2, which yielded a smaller value than dDsC. Overall, the ΔC_{44} values were greater than those of ΔC_{11} and ΔC_{12}. Furthermore, our findings are consistent with those of Freire *et al.*[42]

From the elastic constants, we can calculate other bulk properties such as the bulk modulus (B), Young's modulus (E), and shear modulus (G), which can be calculated using Hill's equations,[43]

$$B = (C_{11} + 2C_{12})/3, \quad (4)$$

$$G = (C_{11} - C_{12} + 3C_{44})/5, \quad (5)$$

$$E = 9GB/(G + 3B). \quad (6)$$

The bulk modulus of a material reveals its resistance to compression, while the Young's modulus represents its stiffness or resistance to elastic deformation under load, and the shear modulus indicates the response of the material to shear stress. The variation of the data calculated using PBE with respect to the experimental reference ranges from −9.02% to 1.73%. When vdW corrections were used, all mechanical properties increased in magnitude. This is also a consequence of the attractive character of vdW interactions, which affects the shape of the potential energy surface near the equilibrium. The vdW corrections increase the interaction between atoms in the crystal, making the material more difficult to deform. The only exception to this observation is that the TS+SCS method decreased the Young's modulus and shear modulus. For the variations in relation to PBE, the trend established for C_{11}, C_{12}, and C_{44} was observed again. Furthermore, the values of ΔB were lower than the values of ΔE and ΔG.

3.2 Clean surface properties

The properties for the clean Cu(111) surface are summarized in Table 2, while their relative change compared to the value obtained with PBE are depicted in Fig. 3.

3.2.0.1 Surface energy. The surface energy is the energy required to separate an infinite crystal into two semi-infinite crystals, calculated as,[20,44]

$$\gamma = (E_{tot}^{slab} - N_I E_{tot}^{bulk})/2A, \quad (7)$$

Table 2 Effect of the vdW corrections on the properties of the clean Cu(111) surface: surface energy (γ), work function (Φ), interlayer spacing relaxations (Δd_{ij}), and d-band center (ε_d^i)

DFT	γ (J m^{-2})	Φ (eV)	Δd_{12} (%)	Δd_{23} (%)	Δd_{34} (%)	ε_d^1 (eV)	ε_d^2 (eV)	ε_d^3 (eV)
PBE	1.298	4.805	−0.901	−0.293	0.076	−2.463	−2.768	−2.760
PBE+D2	1.997	4.843	0.442	−0.192	−0.136	−2.563	−2.905	−2.918
PBE+D3	2.225	4.854	1.003	−0.083	−0.248	−2.556	−2.900	−2.922
PBE+D3(BJ)	2.231	4.849	0.667	−0.092	−0.197	−2.563	−2.906	−2.923
PBE+TS	2.559	4.857	1.579	−0.006	−0.288	−2.589	−2.944	−2.976
PBE+TS+SCS	0.892	4.806	−1.155	−2.267	−2.396	−2.502	−2.846	−2.891
PBE+TS+HI	2.526	4.862	1.478	−0.007	−0.266	−2.587	−2.940	−2.970
PBE+dDsC	1.817	4.815	−0.038	−0.046	−0.051	−2.527	−2.850	−2.852
Expt.	1.825[40]	4.98[41]	—	—	—	—	—	—

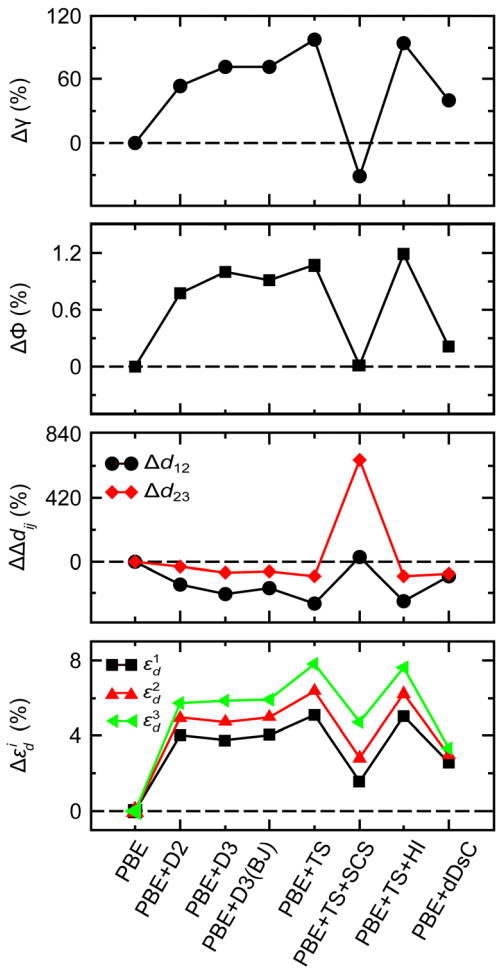

Fig. 3 Relative changes in the surface Cu(111) properties compared to the PBE results: surface energy ($\Delta\gamma$), work function ($\Delta\Phi$), interlayer spacing relaxations ($\Delta\Delta d_{ij}$), and d-band center ($\Delta\varepsilon_d^i$). The dashed lines indicate the PBE results, respectively.

where A is the cross-sectional area of the slab using a (1×1) unit cell. N_l is the number of layers in the slab, E_{tot}^{slab} is the total energy of the slab, and E_{tot}^{bulk} is the total energy of the bulk unit cell.

In line with previous studies,[20,44] we found that PBE underestimates the surface energy by 28.85% when compared to experimental results given by Boer *et al.*[40] Accurate measurements of surface energies are often indirect and subject to many systematic errors,[45] such as the presence of impurities and the difficulty in distinguishing between different surface terminations. Except for the PBE+TS+SCS scheme, the use of the selected vdW corrections led to an increase in the surface energy. The rise in γ is related with the increased value of the cohesion energy in the bulk phase produced by the addition of the vdW corrections, which makes it more difficult to break the crystal cohesion and form a surface. As the surface energy decreases, surface stability increases; therefore, the use of vdW dispersion forces destabilizes the formation of the Cu(111) surface. With the exception of PBE+TS+SCS, the TS schemes had the greatest deviations compared to the PBE results, followed by Grimme's corrections and dDsC correction. The range of $\Delta\gamma$ values is between −31.34% for PBE+TS+SCS and 97.10% for PBE+TS.

3.2.0.2 Work function. The work function (Φ) is the energy necessary to remove an electron from the surface of the solid to a distant point in the vacuum region, expressed as,[46]

$$\Phi = V_{es}(r_{vac}) - E_{Fermi}, \quad (8)$$

where $V_{es}(r_{vac})$ is the electrostatic potential in the middle of the vacuum region of the slab unit cell and E_{Fermi} is the Fermi energy. Using PBE, we obtained a work function of 4.805 eV, which is in good agreement with the experimental value of 4.98 eV determined by Michaelson.[41] As shown in Table 2, the addition of the vdW correction results in a slight increase in the work function, but the variation is less than 1.20% compared with the PBE value. Thus, the contribution of vdW dispersion forces is minimal, as the work function is predominantly influenced by the chemical species present in the substrate and the electrostatic potential far from the surface.[1,42,44,46,47]

3.2.0.3 Interlayer spacing relaxations. Surface atoms have smaller coordination number than bulk atoms, and hence, the distance between the atomic layers on the surface differs from the bulk values.[44,46] The interlayer spacing relaxations (Δd_{ij}) can be determined by the following equation,

$$\Delta d_{ij} = 100(d_{ij} - d_0)/d_0, \quad (9)$$

where d_{ij} is the vertical interlayer spacing distance between layers i and j, and d_0 indicates the vertical interlayer spacing distance between layers in the bulk phase. As observed in previous studies,[44] PBE yields tiny contractions for the two

topmost interlayer spacings. Only the TS+SCS and dDsC vdW corrections yielded contractions for the interlayer spacing; however, TS+SCS resulted in roughly identical contractions for all layers, *i.e.*, it does not exhibit the expected oscillatory decrease in the magnitude of the changes. Therefore, it results in a qualitatively incorrect behavior for interlayer relaxations. In contrast, the remaining vdW corrections result in an increase in the interlayer spacing of the uppermost layer, which can be explained as a consequence of the contraction of the lattice parameter. That is, a lateral strain in the slab implied an expansion toward the vacuum region. Except for TS+SCS, the remaining vdW corrections resulted in tiny contractions for the second interlayer spacing.

3.2.0.4 d-band center. The d-band center is an important concept in adsorption studies and has been widely used to understand activity trends in metal surface-catalyzed reactions,[48] where a shift toward the Fermi level implies lower substrate stability and stronger adsorption.[4,49,50] A shift in the center of the d-band can lead to the filling of antibonding orbitals in the adsorbed molecules, resulting in dissociative adsorption; however, in this study only molecular adsorption was observed. PBE results for the outermost layers are closer to the Fermi level than those for the innermost layers. The use of vdW corrections induces a shift in the d-band center away from the Fermi level, which can be attributed to the extra compressive strain added to the structure by the vdW dispersion forces.[42,51,52] As a result, the stability of the substrate decreased, which is consistent with the surface energy data calculated in this work. Furthermore, the values obtained with TS corrections differed significantly from the PBE value, followed by Grimme's corrections and dDsC, with the exception of PBE+TS+SCS: $\Delta\varepsilon_d^{TS} > \Delta\varepsilon_d^{Grimmes} > \Delta\varepsilon_d^{dDsC} > \Delta\varepsilon_d^{PBE+TS+SCS}$.

3.3 Adsorption properties

Based on the results obtained for the bulk structure and clean surface, we selected only two vdW corrections (PBE+D3 and PBE+dDsC) for the study of the adsorption properties on the Cu(111) surface. Six distinct adsorbates (CH_3, CH_4, CO, CO_2, OH and H_2O) were considered to investigate the impact of vdW corrections on the adsorption properties. Table 3 and Table 4 summarize these effects for the most stable adsorption sites. Several corrections yielded similar results, which are detailed in the ESI.†

3.3.0.1 Adsorption energy. The adsorption energy (E_{ad}) quantifies the strength of the adsorbate–substrate interaction, which is defined by the following equation,

$$E_{ad} = \frac{1}{2}\left(E_{tot}^{Mol/Sub} - 2E_{tot}^{Mol} - E_{tot}^{Sub}\right), \quad (10)$$

where $E_{tot}^{Mol/Sub}$, E_{tot}^{Mol} and E_{tot}^{Sub} are the total energy of the molecule-substrate, gas-phase molecule, and clean substrate systems, respectively. The terms $\frac{1}{2}$ and 2 are needed when placing adsorbates on both sides of the slab. The stronger the adsorbate–substrate interaction, the smaller E_{ad}. The following trend was discovered in this work: $E_{ad}^{CH_4} > E_{ad}^{CO_2} > E_{ad}^{H_2O} > E_{ad}^{CO} > E_{ad}^{CH_3} > E_{ad}^{OH}$, indicating that the adsorbed radicals had the strongest interaction with the Cu(111) surface, followed by polar and non-polar molecules.

The adsorption energy is closer to zero for systems with adsorbates CO_2, CH_4, and H_2O indicating that these systems are weakly bonded. This is consistent with previous research in the literature.[53] In the case of CO, all simulations suggest that the hollow fcc site is somewhat more stable than the hollow hcp and bridge sites, which is also consistent with earlier research.[2] For OH, the bridge and hollow fcc sites are the most stable with PBE; however, when vdW corrections are taken into account, the hollow fcc site becomes the most stable adsorption site, closely followed by the hollow hcp site. Other studies in the literature indicate that the hollow fcc site is the most stable for OH adsorption.[2] Finally, in the case of CH_3, PBE cannot distinguish between the three most stable sites: bridge, hollow fcc, and hollow hcp. When PBE+D3 is used, the most stable adsorption sites are hollow fcc and hollow hcp, but when PBE+dDsC is used, the most stable adsorption site is hollow hcp. In this case, the literature indicates that the hollow hcp is the most stable site.[2] There are no significant changes between the top and top* configurations, except for OH.

Our findings indicate that site preference for adsorption varies with the vdW dispersion corrections. In fact, the geometry of the chemical system can affect the dispersion corrections in different ways. For example, the coordination number is the main geometric factor that affects the dispersion energy in the D3 framework,[7,12] while in the dDsC scheme, the chemical environment is considered through the dipole moment generated by the XC hole around each atom.[54] As noted above, the specific atomic arrangement can lead to differences in the most stable sites for adsorption. Here, despite the effect of vdW corrections on site preference for adsorption, the same order of adsorption energy was observed for all adsorbed species: $E_{ad}^{PBE} > E_{ad}^{PBE+dDsC} > E_{ad}^{PBE+D3}$. Moreover, the use of vdW corrections decreased the value of E_{ad}, which is also consistent with the attractive nature of the dispersion forces of vdW.

3.3.0.2 Vertical adsorbate–substrate distance. The vertical distance between the adsorbate and the copper surface ($d_{Mol\text{-}Cu}$) is directly proportional to the adsorption energy, *e.g.*, non-polar molecules are weakly bound to the substrate at greater distances from the substrate, whereas strongly bound adsorbates, such as radicals, are observed at shorter distances. The use of the vdW corrections has no effect on the adsorption systems of CO, OH, and CH_3. However, for weakly bound systems, the use of the vdW corrections decreases the value of $d_{Mol\text{-}Cu}$. The greatest discrepancy was observed in the results for CH_4 and H_2O. When PBE and PBE+dDsC are used for CH_4, the variation in $d_{Mol\text{-}Cu}$ between sites is less than 0.05 Å; however, when using PBE+D3, $d_{Mol\text{-}Cu}$ at the hollow fcc site is at least 1.65 Å greater than $d_{Mol\text{-}Cu}$ for the other sites. For H_2O in the absence of vdW corrections, the molecule at the top site is closer to the surface than at the hollow fcc site; however, after applying the vdW corrections, there is almost no difference between the sites.

3.3.0.3 Average bond length and average angle. We calculated the variation in bond lengths (Δd_b) and angles ($\Delta\alpha$) for

Table 3 Adsorption properties for the most stable sites using PBE, PBE+D3 and PBE+dDsC: vertical adsorbate–substrate distance (d_{Mol-Cu}), average bond length (d_b), average bond angle (α), variation in the average bond length (Δd_b) and variation in the average bond angle ($\Delta\alpha$) in relation to the gas-phase molecules, and adsorption energy (E_{ad})

Adsorbate	DFT	Site	d_{Mol-Cu} (Å)	d_b (Å)	Δd_b (%)	α (°)	$\Delta\alpha$ (%)	E_{ad} (eV)
CH_3	PBE	Hollow fcc	1.769	1.108	1.85	105.8	−11.82	−1.527
	PBE+D3	Hollow fcc	1.742	1.106	1.74	106.2	−11.52	−1.917
	PBE+dDsC	Hollow hcp	1.746	1.107	1.79	106.1	−11.59	−1.708
CH_4	PBE	Top*	3.389	1.097	−0.01	109.5	0.00	0.005
	PBE+D3	Bridge	3.079	1.098	0.08	109.5	0.00	−0.276
	PBE+dDsC	Hollow hcp	3.137	1.098	0.06	109.5	0.00	−0.163
CO	PBE	Hollow fcc	1.482	1.178	3.47	—	—	−0.935
	PBE+D3	Hollow fcc	1.492	1.177	3.38	—	—	−1.115
	PBE+dDsC	Hollow fcc	1.475	1.177	2.86	—	—	−1.056
CO_2	PBE	Top	3.546	1.173	0.03	179.9	−0.06	−0.009
	PBE+D3	Bridge	3.198	1.173	0.06	179.8	−0.13	−0.229
	PBE+dDsC	Hollow hcp	3.305	1.173	.03	179.8	−0.10	−0.161
OH	PBE	Hollow fcc	1.364	0.972	−1.31	—	—	−3.089
	PBE+D3	Hollow fcc	1.399	0.972	−1.41	—	—	−3.185
	PBE+dDsC	Hollow fcc	1.381	0.972	−1.39	—	—	−3.125
H_2O	PBE	Top	2.399	0.978	0.72	104.3	0.21	−0.185
	PBE+D3	Top	2.364	0.979	0.81	104.3	0.15	−0.427
	PBE+dDsC	Top*	2.319	0.977	0.65	104.7	0.54	−0.328

Table 4 Adsorption properties for the hollow fcc site using PBE, PBE+D3 and PBE+dDsC: change in work function ($\Delta\Phi$ in eV), and change in the Bader charge of the adsorbate (ΔQ_{Mol} in e) and the substrate (ΔQ_{Sub} in e)

	PBE			PBE+D3			PBE+dDsC		
System	$\Delta\Phi$	ΔQ_{Mol}	ΔQ_{Sub}	$\Delta\Phi$	ΔQ_{Mol}	ΔQ_{Sub}	$\Delta\Phi$	ΔQ_{Mol}	ΔQ_{Sub}
CH_3	−0.57	−0.34	0.34	−0.62	−0.33	0.33	−0.46	−0.30	0.30
CH_4	−0.19	−0.03	0.03	−0.24	−0.03	0.03	−0.24	−0.03	0.03
CO	0.31	−0.36	0.36	0.30	−0.35	0.35	0.33	−0.35	0.35
CO_2	−0.08	−0.04	0.04	−0.15	−0.05	0.05	−0.12	−0.05	0.05
OH	−0.76	−0.59	0.59	−0.79	−0.58	0.58	−0.76	−0.58	0.58
H_2O	−0.02	−0.02	0.02	−0.43	0.00	0.00	−0.51	0.00	0.00

each molecule after adsorption. Except for CH_3, which changed from trigonal planar to trigonal pyramidal, all molecules maintained their gas-phase geometry. The bond length was not affected by the vdW corrections, all deviations compared to PBE remained smaller than 3.50%. The same holds for bond angles in which the variation in relation to PBE was smaller than 0.60%.

3.3.0.4 Work function and Bader charge. All results shown in Table 4 were obtained at the hollow fcc site. The hollow fcc site was chosen because it is the most stable for the adsorption of CO, OH, and CH_3 on the Cu(111) surface, with the exception of when PBE+dDsC is used for the adsorption of CH_3. The change in the work function was calculated as,

$$\Delta\Phi = \Phi^{Mol/Sub} - \Phi^{Sub}, \quad (11)$$

where $\Phi^{Mol/Sub}$ and Φ^{Sub} are the work functions of the adsorbed system and the clean surface, respectively. Except for CO, all values for $\Delta\Phi$ were negative. To better understand the change in the work function, the variation in the effective Bader charge was calculated for the adsorbed molecule (ΔQ_{mol}) and for the substrate (ΔQ_{sub}) in relation to its isolated configurations.[55–57] These results indicate that there is an effective transfer of charge from the substrate to adsorbates, which supports the negative values of the change in the work function. The vdW corrections did not significantly affect the variation in the Bader charge.

4 Conclusions

In this work, the effects of several vdW corrections (D2, D3, D3(BJ), TS, TS+SCS, TS+HI, and dDsC) on the adsorption properties of CH_3, CH_4, CO, CO_2, OH and H_2O on the Cu(111) surface were examined. For the Cu fcc bulk, our results demonstrate that the attractive nature of the vdW interaction reduced the lattice constant and increased the mechanical properties of the material, including elastic constants, and bulk, Young's and shear modulus. The C_{11} and C_{44} elastic constants, on the other hand, decreased when PBE+TS+SCS was used in the calculation. Furthermore, the magnitude of the cohesion energy increases when the vdW corrections were employed, which is also due to the attractive nature of the vdW corrections. The surface energy of Cu(111) increased as a result of the enhancement of the cohesion energy, except for the TS+SCS correction. We also observed a slight shift away from the Fermi level in the d-band center induced by the inclusion of vdW corrections. Regarding interlayer spacing relaxations of the Cu(111) surface, we found that the use of vdW corrections decreases its magnitude, except for TS+SCS, which increased Δd_{12} and Δd_{23}. In fact, TS+SCS yielded unphysical interlayer relaxations for deep layers within the slab. The contribution of vdW correction to the work function is negligible, as Φ is mainly affected by adsorbed chemical species.

Based on the performance of the vdW corrections for the bulk and surfaces, we selected only two vdW corrections (PBE+D3 and PBE+dDsC) for the study of adsorption on the Cu(111) surface. For all adsorbed systems, the adsorption energy and the adsorbate–substrate distance decreased with the inclusion of vdW corrections in the calculation. Our findings also indicate that the atomic arrangement of the chemical system can lead to differences in site preference for adsorption

when different vdW corrections are compared. The strength of the adsorbate–substrate interaction was also reflected in the vertical distance between the adsorbate and substrate. Because CH_3 and OH interact more strongly with the surface, $d_{\text{Mol-Cu}}$ was smaller in these systems than for polar and non-polar molecules. The bond lengths and angles remained relatively unchanged upon adsorption, with the exception of CH_3. From the effective Bader charge analysis, all adsorbed systems had positive charge variations in the substrate (ΔQ_{sub}), indicating an effective charge transfer from the substrate to the adsorbate. This finding is in line with the negative values observed in the work function change. With the exception of CO, all $\Delta\Phi$ values were negative. Furthermore, the use of vdW corrections had a negligible effect on $\Delta\Phi$, ΔQ_{mol}, and ΔQ_{sub}.

Author contributions

Eduardo O. Bartaquim: conceptualization, investigation, formal analysis, writing – original draft; Raquel C. Bezerra: formal analysis, writing – review and editing; Albert F. B. Bittencourt: formal analysis, writing – review and editing, visualization; Juarez L. F. Da Silva: conceptualization, supervision, formal analysis, writing – review and editing.

Conflicts of interest

There are no conflicts to declare.

Acknowledgements

The authors gratefully acknowledge support from FAPESP (São Paulo Research Foundation, Grant Numbers 2017/11631-2 and 2018/21401-7), Shell and the strategic importance of the support given by ANP (Brazil's National Oil, Natural Gas and Biofuels Agency) through the R&D levy regulation, and from National Council for Scientific and Technological Development (CNPq, Grant Numbers 143375/2019-9 and 131210/2021-1). The authors also thank the Department of Information Technology – Campus São Carlos, for hosting our cluster.

References

1 R. L. H. Freire, A. Kiejna and J. L. F. Da Silva, *Phys. Chem. Chem. Phys.*, 2016, **18**, 29526–29536.
2 L. Xu, J. Lin, Y. Bai and M. Mavrikakis, *Top. Catal.*, 2018, **61**, 736–750.
3 A. Dabrowski, *Adv. Colloid Interface Sci.*, 2001, **93**, 135–224.
4 J. K. Nørskov, A.-P. Frank, S. Felix and B. Thomas, *Proc. Natl. Acad. Sci. U. S. A.*, 2011, **108**, 937–943.
5 E. R. Johnson, I. D. Mackie and G. A. DiLabio, *J. Phys. Org. Chem.*, 2009, **22**, 1127–1135.
6 S. Grimme, *Wiley Interdiscip. Rev.: Comput. Mol. Sci.*, 2011, **1**, 211–228.
7 J. Klimeš and A. Michaelides, *J. Chem. Phys.*, 2012, **137**, 120901.
8 M. Dion, H. Rydberg, E. Schröder, D. C. Langreth and B. I. Lundqvist, *Phys. Rev. Lett.*, 2004, **92**, 246401.
9 K. Lee, É. D. Murray, L. Kong, B. I. Lundqvist and D. C. Langreth, *Phys. Rev. B: Condens. Matter Mater. Phys.*, 2010, **82**, 081101.
10 S. Grimme, *J. Comput. Chem.*, 2006, **27**, 1787–1799.
11 J.-D. Chai and M. Head-Gordon, *Phys. Chem. Chem. Phys.*, 2008, **10**, 6615–6620.
12 S. Grimme, J. Antony, S. Ehrlich and H. Krieg, *J. Chem. Phys.*, 2010, **132**, 154104.
13 S. Grimme, S. Ehrlich and L. Goerigk, *J. Comput. Chem.*, 2011, **32**, 1456–1465.
14 A. Tkatchenko and M. Scheffler, *Phys. Rev. Lett.*, 2009, **102**, 073005.
15 A. Tkatchenko, R. A. DiStasio, R. Car and M. Scheffler, *Phys. Rev. Lett.*, 2012, **108**, 236402.
16 T. Bučko, S. Lebègue, J. Hafner and J. G. Ángyán, *J. Chem. Theory Comput.*, 2013, **9**, 4293–4299.
17 T. Bučko, S. Lebègue, J. G. Ángyán and J. Hafner, *J. Chem. Phys.*, 2014, **141**, 034114.
18 S. N. Steinmann and C. Corminboeuf, *J. Chem. Phys.*, 2011, **134**, 044117.
19 S. N. Steinmann and C. Corminboeuf, *J. Chem. Theory Comput.*, 2011, **7**, 3567–3577.
20 J. L. F. Da Silva, C. Barreteau, K. Schroeder and S. Blügel, *Phys. Rev. B: Condens. Matter Mater. Phys.*, 2006, **73**, 125402.
21 S. E. Allen, R. R. Walvoord, R. Padilla-Salinas and M. C. Kozlowski, *Chem. Rev.*, 2013, **113**, 6234–6458.
22 Y. Tsuji and T. Fujihara, *Sustainable Catalysis: With Non-endangered Metals, Part 2*, The Royal Society of Chemistry, 2015, ch. 15, pp.1–40.
23 Z. Zuo, P. J. Ramírez, S. D. Senanayake, P. Liu and J. A. Rodriguez, *J. Am. Chem. Soc.*, 2016, **138**, 13810–13813.
24 E. Huang, I. Orozco, P. J. Ramírez, Z. Liu, F. Zhang, M. Mahapatra, S. Nemsšaák, S. D. Senanayake, J. A. Rodriguez and P. Liu, *J. Am. Chem. Soc.*, 2021, **143**, 19018–19032.
25 P. Hohenberg and W. Kohn, *Phys. Rev.*, 1964, **136**, B864–B871.
26 W. Kohn and L. J. Sham, *Phys. Rev.*, 1965, **140**, A1133–A1138.
27 G. Kresse and J. Hafner, *Phys. Rev. B: Condens. Matter Mater. Phys.*, 1993, **48**, 13115–13118.
28 G. Kresse and J. Furthmüller, *Phys. Rev. B: Condens. Matter Mater. Phys.*, 1996, **54**, 11169–11186.
29 G. Kresse and D. Joubert, *Phys. Rev. B: Condens. Matter Mater. Phys.*, 1999, **59**, 1758–1775.
30 J. P. Perdew, K. Burke and M. Ernzerhof, *Phys. Rev. Lett.*, 1996, **77**, 3865–3868.
31 P. E. Blöchl, *Phys. Rev. B: Condens. Matter Mater. Phys.*, 1994, **50**, 17953–17979.
32 H. J. Monkhorst and J. D. Pack, *Phys. Rev. B: Condens. Matter Mater. Phys.*, 1976, **13**, 5188–5192.
33 J. M. Morbec and P. Kratzer, *J. Chem. Phys.*, 2017, **146**, 034702.
34 A. D. Becke and E. R. Johnson, *J. Chem. Phys.*, 2005, **123**, 154101.
35 M. E. Straumanis and L. S. Yu, *Acta Crystallogr., Sect. A: Cryst. Phys., Diffr., Theor. Gen. Crystallogr.*, 1969, **25**, 676–682.

36 D. A. Young, *Phase Diagrams of the Elements*, University of California Press, Ewing, NJ, USA, 2020, pp. 168–195.
37 J. R. Rumble, *CRC Handbook of Chemistry and Physics*, CRC Press, Taylor & Francis, 102nd Edition (Internet Version 2021), 2021.
38 L. B. Freund and S. Suresh, *Thin Film Materials: Stress, Defect Formation and Surface Evolution*, Cambridge University Press, Cambridge, England, UK, 2004.
39 H. M. Ledbetter, *J. Phys. D: Appl. Phys.*, 1980, **13**, 1879–1884.
40 F. R. de Boer, W. C. M. Mattens, R. Boom, A. R. Miedema and A. K. Niessen, *Cohesion in Metals: Transition Metal Alloys*, North-Holland, 1988.
41 H. B. Michaelson, *J. Appl. Phys.*, 1977, **48**, 4729–4733.
42 R. L. H. Freire, D. Guedes-Sobrinho, A. Kiejna and J. L. F. Da Silva, *J. Phys. Chem. C*, 2018, **122**, 1577–1588.
43 R. Hill, *Proc. Phys. Soc., London, Sect. A*, 1952, **65**, 349–354.
44 J. L. F. Da Silva, C. Stampfl and M. Scheffler, *Surf. Sci.*, 2006, **600**, 703–715.
45 P. Lazar and M. Otyepka, *Phys. Rev. B: Condens. Matter Mater. Phys.*, 2015, **91**, 115402.
46 J. L. F. Da Silva, *Phys. Rev. B: Condens. Matter Mater. Phys.*, 2005, **71**, 195416.
47 R. L. H. Freire, A. Kiejna and J. L. F. Da Silva, *J. Phys. Chem. C*, 2014, **118**, 19051–19061.
48 I. Takigawa, K.-i Shimizu, K. Tsuda and S. Takakusagi, *RSC Adv.*, 2016, **6**, 52587–52595.
49 B. Hammer and J. K. Nørskov, *Advances in Catalysis*, Academic Press, Cambridge, MA, USA, 2000, vol. 45, pp.71–129.
50 B. Hammer and J. K. Nørskov, *Nature*, 1995, **376**, 238–240.
51 J. R. Kitchin, J. K. Nørskov, M. A. Barteau and J. G. Chen, *Phys. Rev. Lett.*, 2004, **93**, 156801.
52 F. Calleja, V. M. García-Suárez, J. J. Hinarejos, J. Ferrer, A. L. V. de Parga and R. Miranda, *Phys. Rev. B: Condens. Matter Mater. Phys.*, 2005, **71**, 125412.
53 P. C. D. Mendes, V. K. Ocampo-Restrepo and J. L. F. Da Silva, *Phys. Chem. Chem. Phys.*, 2020, **22**, 8998–9008.
54 T. Risthaus and S. Grimme, *J. Chem. Theory Comput.*, 2013, **9**, 1580–1591.
55 R. F. W. Bader, *Atoms in Molecules: A Quantum Theory*, Clarendon Press, 1994.
56 W. Tang, E. Sanville and G. Henkelman, *J. Phys.: Condens. Matter*, 2009, **21**, 084204.
57 G. Henkelman, A. Arnaldsson and H. Jónsson, *Comput. Mater. Sci.*, 2006, **36**, 354–360.

